Journal of Solid State Chemistry 207 (2013) 69–79

Contents lists available at ScienceDirect

Journal of Solid State Chemistry

journal homepage: www.elsevier.com/locate/jssc

Synthesis and structural and magnetic characterization of the frustrated magnetic system $La_2Ni_{4/3-x}Co_xSb_{2/3}O_6$

D.G. Franco [a,b,*], R.E. Carbonio [b,1], G. Nieva [a,c,1]

[a] Laboratorio de Bajas Temperaturas, Centro Atómico Bariloche (CNEA), 8400 Bariloche, Río Negro, Argentina
[b] INFIQC-CONICET, Dpto. de Físico-Química, Facultad de Ciencias Químicas, Universidad Nacional de Córdoba, Ciudad Universitaria, X5000HUA Córdoba, Argentina
[c] Instituto Balseiro (CNEA-UNCuyo) Centro Atómico Bariloche, 8400 Bariloche, Río Negro, Argentina

ARTICLE INFO

Article history:
Received 18 June 2013
Received in revised form
12 August 2013
Accepted 8 September 2013
Available online 21 September 2013

Keywords:
Double perovskites
Neutron diffraction
Rietveld refinement
Ferrimagnetism
Magnetic frustration

ABSTRACT

We report the synthesis of double perovskites $La_2Ni_{4/3-x}Co_xSb_{2/3}O_6$ with $x=0$, 1/3, 2/3 and 1 by a solid state method. Rietveld refinements of X-ray and neutron powder diffraction data show that all samples crystallize in space group $P2_1/n$, with almost perfect occupation of the 2*d* octahedral site with the transition metals, while all Sb^{5+} are randomly distributed in a 2*c* octahedral site. The saturation magnetization in hysteresis loops indicates that the samples are ferrimagnetic throughout all the series. Virgin magnetization curves lie outside hysteresis loops at low temperatures and thermal evolution of H_m – defined as the inflection point of these curves – follows the de Almeida–Thouless dependence for $x \neq 0$. This spin glass like behavior below 30 K is also supported by thermal evolution of the coercivity, which follows an exponential law typical of magnetic clusters, not found in the pure Ni^{2+} perovskite, $x=0$ extreme.

1. Introduction

Pioneer work in magnetic perovskites $AMnO_3$ near room temperature was done more than sixty years ago [1]. In the following decades rhenium [2] and molybdenum and tungsten [3] perovskites were studied. However, renewed interest emerged in the last few years as new properties were reported: high temperature superconductivity in Ba–LaCu–O [4], colossal magnetoresistance in $La_{0.67}Ca_{0.33}MnO_x$ thin films [5] and *half-metal* properties in Sr_2FeMoO_6 [6], with potential applications in *spintronics*, just to name three examples.

General formula for perovskite oxides is ABO_3, where *A* is usually an alkali-earth ion and *B* a transition metal. The ideal cubic structure can be constructed as a three dimensional array of corner sharing *B* O_6 octahedra with *A* cations placed at cuboctahedral sites between eight *B* O_6 octahedra. The structure is highly versatile and can accommodate almost any element in *A* and/or *B* sites, and also more than one in each site. This explains the wide spectrum of physical phenomena found in perovskite systems and drives the search for new materials and properties.

Two different *B* ions placed in the structure can occupy two octahedral sites, usually in a rock salt pattern [7], and then the perovskite is double. The degree of order depends on several factors [8], but the order is mainly favored when the differences in size and charge between the involved cations are large. Besides, the different sizes of *A* and *B* cations can lead to important structural distortions. It has been shown in some systems that the degree of order and distortions strongly affect the physical properties [9–11].

Because many studied systems have equal amounts of two *B* ions it has become common use to write the formula of double perovskites as $A_2BB'O_6$. In this case, if only *B* has unpaired electrons and the order is maximum, this is all *B* cations placed at one octahedral site and the other site fully occupied by *B′*, interactions occur only through super-superexchange *B*–O–*B′*–O–*B* paths, usually antiferromagnetic in nature. Because of the long distance between *B* ions, transition temperatures T_N are frequently low. In this picture disorder introduces superexchange *B*–O–*B* interactions, antiferromagnetic or ferromagnetic according to the number of unpaired electrons and bond angle [12] – among other factors – and also intriguing magnetic phenomena, like spin glass behavior, formation of magnetic clusters, and frustration [13–16].

Another approach for the emergence of interesting magnetic properties is the design of new materials with different B/B' proportion. Few reports of $A_2B_{4/3}B'_{2/3}O_6$ double perovskites are found in bibliography. The particularity of this stoichiometry is that even the most ordered situation has superexchange

* Corresponding author at: Laboratorio de Bajas Temperaturas, Centro Atómico Bariloche (CNEA), Av. E. Bustillo 9500, S. C. de Bariloche, 8400 Río Negro, Argentina. Tel.: +54 2944445171; fax: +54 2944445299.
E-mail address: diego.g.franco@cab.cnea.gov.ar (D.G. Franco).
[1] Members of the Research Career of CONICET.

0022-4596/$ - see front matter © 2013 Elsevier Inc. All rights reserved.
http://dx.doi.org/10.1016/j.jssc.2013.09.011

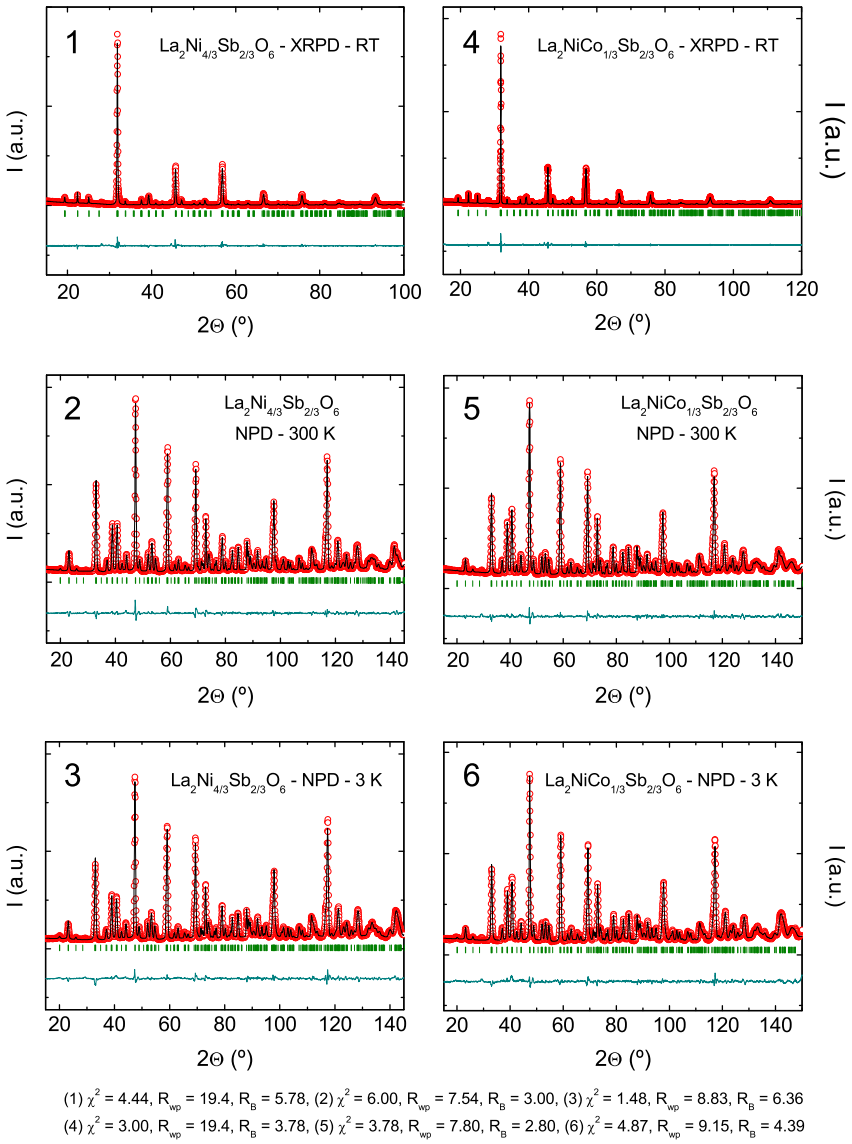

Fig. 1. Rietveld refinement in monoclinic space group $P2_1/n$ for $La_2Ni_{4/3}Sb_{2/3}O_6$ (left) and $La_2NiCo_{1/3}Sb_{2/3}O_6$ (right) of X-ray powder diffraction at room temperature (top, XRPD – RT) and neutron powder diffraction at 300 K (middle, NPD – 300 K) and 3 K (bottom, NPD – 3 K) data. Observed (circles), calculated (black line), difference (bottom line) and Bragg reflections (vertical bars).

interactions, originated by an octahedral site fully occupied by B and the other site with 1/3 of B and 2/3 of B'. Therefore a coexistence of different magnetic interactions occurs and competition between them may lead to a complex magnetic behavior.

Previously, a frustrated magnetic state at low temperatures was informed for $La_2Ni_{4/3}Sb_{2/3}O_6$ [17,18]. Also the synthesis, structure and magnetic properties of the double perovskite $La_2Co_{4/3}Sb_{2/3}O_6$ were reported [19]. Here we present the crystal structure of $La_2Ni_{4/3}Sb_{2/3}O_6$, which was not detailed before, and also the synthesis and crystal structure of three solid solutions between the perovskite with only Ni^{2+} or Co^{2+}: $La_2Ni_{4/3-x}Co_xSb_{2/3}O_6$, where $x=1/3$, 2/3 and 1. The magnetic properties of the double perovskites with nickel and cobalt are also studied and compared with the end members of the family.

2. Materials and methods

Polycrystalline samples of $La_2Ni_{4/3-x}Co_xSb_{2/3}O_6$ with $x=0$, 1/3, 2/3, 1 and 4/3 were synthesized by the solid state method from La_2O_3, NiO, Co_3O_4 and Sb_2O_3 in stoichiometric amounts. The powder mixture was ground and fired first at 950 °C for 12 h in an air atmosphere to avoid antimony losses, given the low melting point of Sb_2O_3 (625 °C). A second treatment at 1400 °C, also for 12 h in the air atmosphere, was performed to obtain the single and crystalline desired phases.

The crystal structure was analyzed from X-ray (XRPD) and neutron (NPD) powder diffraction patterns. XRPD patterns were measured at room temperature on a PANalytical X'Pert PRO diffractometer in Bragg–Brentano geometry with 40 kV, 40 mA and Cu $K\alpha$ radiation of wavelength $\lambda=1.5418$ Å. The scanned angular range was $5^\circ<2\Theta<120^\circ$ with a step size of 0.02°. NPD patterns were collected at 300 and 3 K in vanadium cans in high resolution diffractometer D2B at Institute Laue-Langevin, Grenoble, France. The wavelength used was $\lambda=1.5940$ Å, $0^\circ<2\Theta<160^\circ$ and the step size was 0.05° in all the experiments.

Structure refinement of the diffraction data was performed using the Rietveld method [20] with Fullprof program [21]. In all cases a pseudo-Voigt function leads to good fits of the observed peaks. Background levels were estimated by interpolation between regions of the diffraction pattern where there were no peaks. The refined parameters were zero-point error, scale factor,

background points, cell parameters, profile parameters, asymmetry, *xyz* positions of the different ions, isotropic thermal factors (B_{iso}) and occupation of the different sites.

Measurements of magnetization (M) as a function of temperature (T) and magnetic field (H) were performed in a QD-MPMS squid magnetometer between 5 and 300 K and ± 50 kOe. Usually, a zero field and field cooling (ZFC-FC) procedure was utilized, i.e. cooling with a zero applied field and with a non-zero constant field.

3. Results and discussion

3.1. Crystal structure

XRPD patterns for $La_2Ni_{4/3-x}Co_xSb_{2/3}O_6$ with $x=0$, 1/3, 2/3 and 1 at room temperature showed good crystallinity and the observed reflections for all the compositions are justified by a monoclinic cell space group $P2_1/n$ (#14). However, $La_2Ni_{4/3}Sb_{2/3}O_6$ ($x=0$) was previously informed as $LaNi_{2/3}Sb_{1/3}O_3$ with an orthorhombic simple perovskite structure, space group *Pbnm* (#62) [22].

The major difference between these two structures is the arrangement of the octahedral ions: while the orthorhombic lattice has a random distribution (that is why this model is a simple perovskite), the monoclinic space group has a rock salt one, with two crystallographic sites. Being $P2_1/n$ a subgroup of *Pbnm*, they share several systematic absences, but due to the different array of octahedral ions, space group *Pbnm* has a systematic absence for 0*kl*: $k=2n+1$ which is lifted in the monoclinic space group $P2_1/n$ [23].

The Rietveld refinements performed with the orthorhombic cell were reasonably good, although some peaks were simulated with zero intensity. On the other hand, the monoclinic cell justifies all the experimental peaks, even those that the orthorhombic cell did not. In fact, in the monoclinic model these peaks correspond to 0*kl* with $k=2n+1$ reflections that are prohibited like it was stated before in the space group *Pbnm*. Then, the samples crystallize effectively in a monoclinic cell with a rock salt like arrangement of *B* ions, that is, a double perovskite structure.

In Figs. 1 and 2, Rietveld refinements of XRPD and NPD data for $La_2Ni_{4/3-x}Co_xSb_{2/3}O_6$ ($x=0$, 1/3, 2/3 and 1) are presented with the reliability factors, which are in all cases very good and are defined as follows:

$$\chi^2 = \left[\frac{R_{wp}}{R_{\exp}}\right]^2 \tag{1}$$

$$R_{wp} = 100\left[\frac{\sum_{i,n} w_i |y_{i,obs} - y_{i,cal}|^2}{\sum_{i,n} w_i |y_{i,obs}|^2}\right]^{1/2} \tag{2}$$

$$R_{\exp} = 100\left[\frac{n-p+c}{\sum_i w_i y_{i,obs}^2}\right]^{1/2} \tag{3}$$

$$R_{Bragg} = 100\frac{\sum_k |I_{k,obs} - I_{k,cal}|}{\sum_k |I_{k,obs}|} \tag{4}$$

where w_i is the weight of the observation and is calculated as $w_i = 1/y_{i,obs}$. $y_{i,obs}$ is the diffracted intensity and $y_{i,cal}$ the calculated intensity, both at the angle *i*. *n* is the total number of points used in the refinement (n=total number of points in the pattern minus total number of excluded points). p is the number of refined parameters and c the number of restrictions. $n-p+c$ is the number of degrees of freedom. $I_{k,obs}$ and $I_{k,cal}$ are the observed and calculated integrated intensities respectively corresponding to the k reflection.

Neutron diffraction patterns could also be refined in space group $P2_1/n$, at 300 and 3 K as well, showing on one hand that XRPD conclusions about the quality of the monoclinic model faced to the orthorhombic one was correct, and on the other hand that no structural transition occurs down to 3 K. Besides, no additional peaks at low temperature are observed, disregarding the presence of magnetic long range order.

Lattice parameters and cell volume obtained from refinements of NPD data are presented in Table 1, and the evolution of *a*, *b* and *c* with cobalt content (x) is plotted in Fig. 3. It is evident that the increase in cobalt content expands the cell dimensions, in good agreement with the ionic radii of $^{VI}Ni^{2+}$ and $^{VI}Co^{2+}$ (HS), 0.83 Å and 0.885 Å respectively [24]: the replacement of the Ni^{2+} ion by a bigger one, Co^{2+}, enlarges the unit cell. Also, a compression of the cell is observed at low temperature, with respect to room temperature.

Table 2 shows Wyckoff sites, atomic positions *xyz* and isotropic thermal factors B_{iso}, obtained from the Rietveld refinements of the NPD data, at 300 and 3 K. We can observe that the space group $P2_1/n$ has one site for the *A* ion (La^{3+}), two sites for *B* ions (Ni^{2+}, Co^{2+} and Sb^{5+}) and three different sites for oxygen.

Given that the structure has two crystallographic sites for octahedral ions, 2*d* (1/2, 0, 0) and 2*c* (0, 1/2, 0), we performed the refinement of their occupation at fixed stoichiometry. For $x=0$, where there are two *B* ions, we used NPD refinements only, while for the cases where there are three *B* ions, $x=1/3$, 2/3 and 1, we combined XRPD and NPD refinements, in the way explained as follows.

On one hand, since the difference between X-ray scattering lengths for a first row transition metal and Sb^{5+} is substantial, and considering that Ni^{2+} and Co^{2+} are indistinguishable for X-rays due to their small electronic difference, we performed the refinement of 2*d* and 2*c* sites occupation considering that we had only two octahedral ions: Ni^{2+} (or Co^{2+}) and Sb^{5+}, in 2:1 proportion.

On the other hand, neutron scattering lengths for nickel and cobalt are different enough (1.03 and 0.249×10^{-12} cm respectively) to distinguish them. Then we refined in NPD patterns the distribution of Ni^{2+} and Co^{2+} among 2*d* and 2*c* sites, keeping Sb^{5+} occupations fixed at the values obtained from XRPD refinements, and with the adequate proportion of Ni^{2+}/Co^{2+}: 3/1, 1/1 and 1/3 for $x=1/3$, 2/3 and 1 respectively. In Table 3 we show the results obtained. The distribution of transition metal ions and antimony among 2*d* and 2*c* sites as a function of cobalt content (x) is plotted in Fig. 4, where we defined $M^{2+} = Ni^{2+} + Co^{2+}$.

The most ordered situation for our samples is $La_2(M)_{2d}(M_{1/3}Sb_{2/3})_{2c}O_6$, a scenario which has an intrinsic disorder: 2*d* site is fully occupied by M^{2+}, but 2*c* site has M^{2+} as well as Sb^{5+}, distributed randomly. The opposite situation, a scenario of complete disorder, is $La_2(M_{2/3}Sb_{1/3})_{2d}(M_{2/3}Sb_{1/3})_{2c}O_6$. Looking at Fig. 4 it can be noticed that all double perovskites are highly ordered, as it is expected from the large charge difference between M^{2+} and Sb^{5+}, i.e. 3. Moreover, the increasing degree of order with (x) can be explained based on the ionic radius for $^{VI}Sb^{5+}$, $^{VI}Ni^{2+}$ and $^{VI}Co^{2+}$ (HS), which are 0.74, 0.83 and 0.885 Å respectively. The replacement of Ni^{2+} for a larger ion, Co^{2+}, implies a higher difference between the mean radius of M^{2+} and Sb^{5+} radius, and thus a higher degree of order. According to this tendency, the double perovskite $La_2Co_{4/3}Sb_{2/3}O_6$ ($x=4/3$) is totally ordered [19]. Regarding the distribution of Ni^{2+} and Co^{2+}, due to the same charge and similar radii, no special distribution of them among 2*d* and 2*c* sites is found.

We also refined the occupation of oxygen sites. However the results obtained did not deviate from the stoichiometric values, within the standard deviations. Because of this, the oxygen occupations were finally fixed at their maximum values.

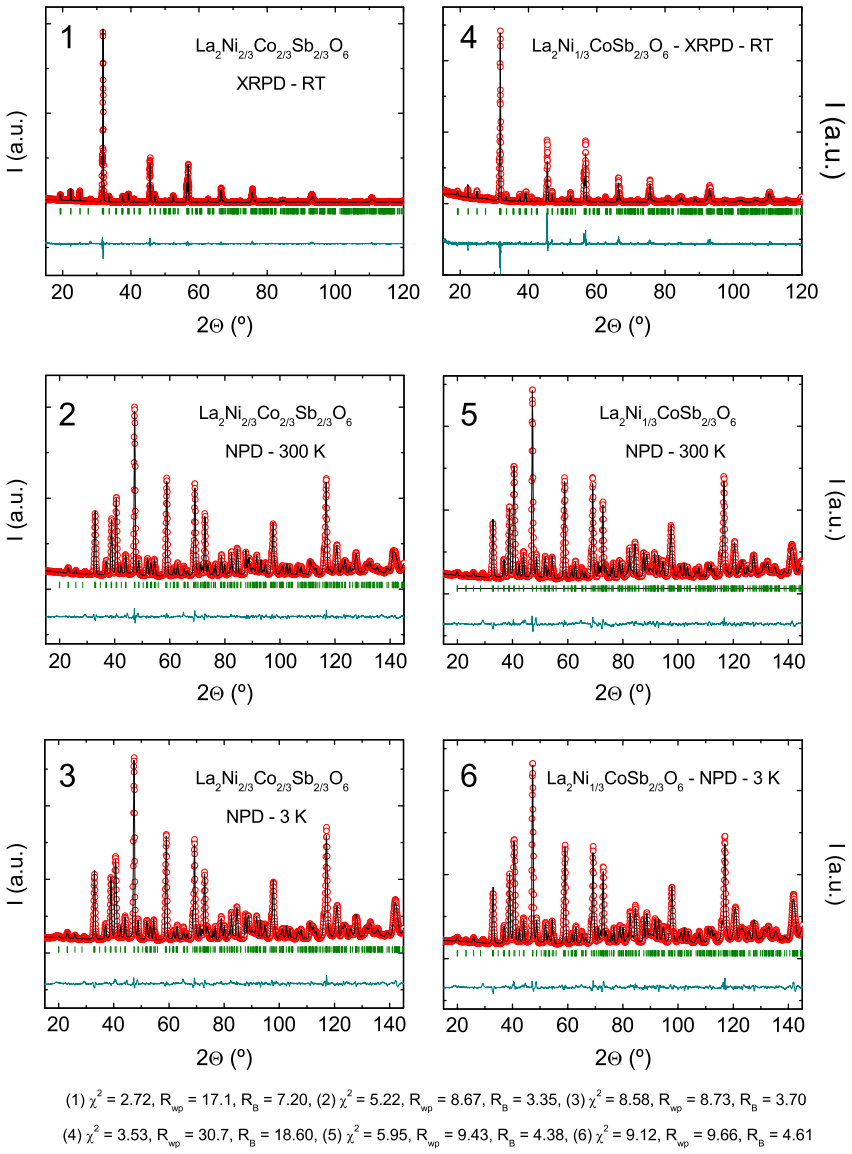

Fig. 2. Rietveld refinement in monoclinic space group $P2_1/n$ for $La_2Ni_{2/3}Co_{2/3}Sb_{2/3}O_6$ (left) and $La_2Ni_{1/3}CoSb_{2/3}O_6$ (right) of X-ray powder diffraction at room temperature (top, XRPD – RT) and neutron powder diffraction at 300 K (middle, NPD – 300 K) and 3 K (bottom, NPD – 3 K) data. Observed (circles), calculated (black line), difference (bottom line) and Bragg reflections (vertical bars).

Table 1
Cell parameters and cell volume V for monoclinic double perovskites $La_2Ni_{4/3-x}Co_xSb_{2/3}O_6$, where $x=0$, 1/3, 2/3 and 1, as obtained from Rietveld refinement of neutron diffraction data at 300 and 3 K.

x	T (K)	a (Å)	b (Å)	c (Å)	β (°)	V (Å^3)
0	300	5.59851(9)	5.63901(9)	7.9293(1)	89.981(2)	250.329(7)
	3	*5.5850(1)*	*5.6353(1)*	*7.9134(2)*	*89.945(1)*	*249.062(9)*
1/3	300	5.6013(1)	5.6420(1)	7.9336(2)	89.988(3)	250.722(8)
	3	*5.5898(1)*	*5.6396(1)*	*7.9193(2)*	*90.026(3)*	*249.65(1)*
2/3	300	5.6016(1)	5.6535(1)	7.9386(2)	89.988(2)	251.406(9)
	3	*5.5898(1)*	*5.6519(1)*	*7.9235(2)*	*89.978(2)*	*250.32(1)*
1	300	5.6046(1)	5.6626(1)	7.9437(2)	89.994(2)	252.11(1)
	3	*5.5931(1)*	*5.6617(1)*	*7.9280(2)*	*89.978(2)*	*251.05(1)*

In Table 4 we show B_{2d}–O and B_{2c}–O distances, as well as B_{2d}–O–B_{2c} bond angles (Θ). As it can be seen Θ values are not 180°, that is there is a tilting of the octahedra, one of the three typical distortions found in perovskite like systems. This effect is attributed to the small radius of the A ion for the cuboctahedral site, 1.5 Å for $^{XII}La^{3+}$ [24]. The distortion optimizes the anion coordination around the La^{3+} ion, by shortening eight of the twelve La–O distances. The tilt angles, defined as $\delta=(\Theta-180°)/2$, are of the same order for all the double perovskites, because Θ is similar for all the compositions (δ values not shown). For space group $P2_1/n$ the tilt system is $a^-a^-c^+$, Fig. 5, in the Glazer notation.

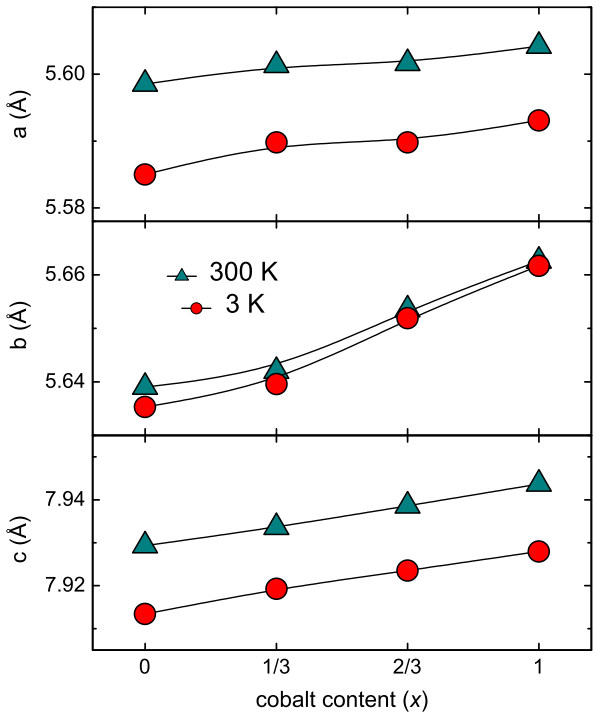

Fig. 3. Evolution of cell parameters *a*, *b* and *c* of double perovskites $La_2Ni_{4/3-x}Co_xSb_{2/3}O_6$ with cobalt content (*x*) at 300 and 3 K. The lines are guides to the eye.

Bond Valence Sums obtained from phenomenological Brown's Bond Valence Model [25] give an estimation of the valence of the different ions in the structure, Table 5. The agreement between the expected oxidation states and the obtained ones is very good for all the ions. It should be noticed that for 2*d* and 2*c* sites the situation is more complex than for La^{3+} and O^{2-} sites, because the samples have more than one cation in each octahedral site, Table 3. Consequently the values theoretically expected were obtained from the occupations *O* as $2O_{Ni_y^{2+}}+2O_{Co_y^{2+}}+5O_{Sb_y^{5+}}$ with $y=2d$ or $2c$.

3.2. Magnetic characterization

Magnetization as a function of temperature for $La_2Ni_{4/3-x}Co_xSb_{2/3}O_6$ with $x=1/3$, 2/3 and 1 was measured using a ZFC-FC procedure with an applied magnetic field of 1 kOe, Fig. 6 (left axis). A clear ferromagnetic-like behavior is observed at low temperatures and also a noticeable irreversibility between ZFC and FC magnetizations below approximately 30 K. The transition temperature T_C, depicted with dotted lines in Fig. 6, was taken as the minimum in dM/dT vs. T (data not shown). The dependence of T_C on cobalt content (*x*) is shown in the inset of Fig. 6(a), where a clear decrease is observed as the cobalt doping is increased. $T_C(x=0)=98(2)$ K and $T_C(x=4/3)\approx 55$ K were extracted from [17,18] and [19] respectively.

At high temperature (200–300 K) a Curie–Weiss behavior is observed for all samples: $H/M=(T-T_{CW})/C$, where *C* is the Curie constant and T_{CW} the Curie–Weiss temperature. In Fig. 6 (right axis) we show experimental *H/M* vs. *T* curves and the linear fits obtained, and also T_{CW} and μ_e, where μ_e is the effective magnetic moment calculated from *C*. The total theoretical magnetic moment is $\mu_{tt}^2=a\mu_t^2(Ni^{2+})+b\mu_t^2(Co^{2+})$, where the coefficients *a* and *b* are related with the stoichiometric amounts of the transition metal ions, and $\mu_t=g\sqrt{J(J+1)}$. Usually for 3*d* transition metals there is no orbital contribution, then the total theoretical magnetic moment obtained are $\mu_{tt}=3.12$, 3.40 and 3.60 μ_B for $x=1/3$, 2/3 and 1 respectively, which are in good agreement with experimental values, see Fig. 6.

Hysteresis loops at 5 K under ZFC conditions were measured for all samples, Fig. 7. It can be noticed at first sight differences between the loop for $x=0$, the double perovskite with Ni^{2+} only, and the loops for the other samples.

Table 2
Wyckoff sites, atomic positions (*xyz*) and isotropic thermal factors (B_{iso}) for $La_2Ni_{4/3-x}Co_xSb_{2/3}O_6$, where $x=0$, 1/3, 2/3 and 1, at 300 and 3 K, as obtained from Rietveld refinement of neutron diffraction data.

x	Atom	Site	*T* (K)	*x*	*y*	*z*	B_{iso}
0	La	4*e*	300	0.4909(5)	0.5374(2)	0.2511(1)	1.65(2)
			3	0.4909(5)	0.5393(2)	0.251(1)	1.43(2)
	B	2*d*	300	1/2	0	0	0.38(1)
			3				0.33(1)
	B	2*c*	300	0	1/2	0	0.38(1)
			3				0.33(1)
	O	4*e*	300	0.2877(7)	0.2967(5)	0.0423(5)	0.94(7)
			3	0.2873(6)	0.2916(8)	0.0438(5)	0.90(7)
	O	4*e*	300	0.2075(6)	0.7851(5)	0.0424(5)	0.72(7)
			3	0.2056(6)	0.7890(7)	0.0422(5)	0.60(7)
	O	4*e*	300	0.5767(2)	0.9834(2)	0.2515(6)	1.06(2)
			3	0.5789(2)	0.9831(2)	0.2510(5)	0.91(2)
1/3	La	4*e*	300	0.4918(5)	0.5387(2)	0.252(1)	1.65(2)
			3	0.4913(5)	0.5405(2)	0.251(1)	1.47(3)
	B	2*d*	300	1/2	0	0	0.46(1)
			3				0.50(2)
	B	2*c*	300	0	1/2	0	0.46(1)
			3				0.50(2)
	O	4*e*	300	0.2887(8)	0.2959(7)	0.0459(4)	1.22(9)
			3	0.2932(8)	0.2855(7)	0.0436(7)	0.70(1)
	O	4*e*	300	0.2074(7)	0.7867(6)	0.0388(4)	0.74(7)
			3	0.2117(9)	0.7959(7)	0.0423(8)	1.0(1)
	O	4*e*	300	0.5785(2)	0.9838(2)	0.2519(8)	1.02(2)
			3	0.5792(2)	0.9831(2)	0.2511(9)	0.99(2)
2/3	La	4*e*	300	0.4919(5)	0.5398(2)	0.2536(8)	1.33(2)
			3	0.4917(4)	0.5419(2)	0.2524(9)	1.14(2)
	B	2*d*	300	1/2	0	0	0.13(2)
			3				0.20(2)
	B	2*c*	300	0	1/2	0	0.13(2)
			3				0.20(2)
	O	4*e*	300	0.2987(7)	0.3008(7)	0.0396(6)	0.64(9)
			3	0.2975(7)	0.2995(7)	0.0415(8)	0.35(9)
	O	4*e*	300	0.2163(7)	0.7809(7)	0.0449(6)	0.41(8)
			3	0.2150(8)	0.7819(7)	0.0445(8)	0.5(1)
	O	4*e*	300	0.5796(4)	0.9831(3)	0.246(1)	0.93(4)
			3	0.5807(4)	0.9822(3)	0.247(2)	0.84(4)
1	La	4*e*	300	0.4917(4)	0.5398(2)	0.2457(9)	1.48(3)
			3	0.4916(4)	0.5421(2)	0.2465(9)	1.37(3)
	B	2*d*	300	1/2	0	0	0.32(3)
			3				0.32(3)
	B	2*c*	300	0	1/2	0	0.32(3)
			3				0.32(3)
	O	4*e*	300	0.285(1)	0.2993(8)	0.0481(6)	1.0(1)
			3	0.287(1)	0.3013(7)	0.0471(7)	0.7(1)
	O	4*e*	300	0.2024(9)	0.7838(8)	0.0384(6)	0.59(9)
			3	0.203(2)	0.7824(7)	0.0398(7)	0.67(9)
	O	4*e*	300	0.5784(5)	0.9826(3)	0.257(1)	1.08(4)
			3	0.5810(4)	0.9818(3)	0.257(1)	1.04(4)

Table 3
Occupation fractions of octahedral 2*d* and 2*c* sites of double perovskites $La_2Ni_{4/3-x}Co_xSb_{2/3}O_6$, obtained from Rietveld refinement of NPD and XRPD data. For details of the procedure, see the text.

x	2*d* site			2*c* site		
	Ni^{2+}	Co^{2+}	Sb^{5+}	Ni^{2+}	Co^{2+}	Sb^{5+}
0	0.97(1)	0	0.03(1)	0.36(1)	0	0.64(1)
1/3	0.71(1)	0.26(1)	0.03	0.29(1)	0.07(1)	0.64
2/3	0.52(1)	0.46(1)	0.02	0.14(1)	0.21(1)	0.65
1	0.224(8)	0.762(8)	0.014	0.110(8)	0.238(8)	0.652

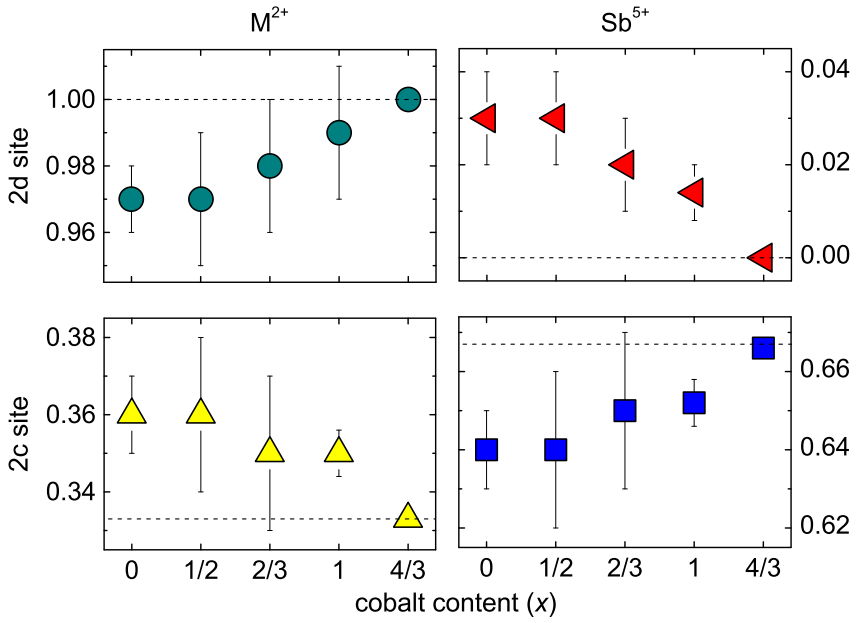

Fig. 4. Occupation of 2*d* (top) and 2*c* (bottom) sites by transition metal M^{2+} (Ni^{2+} + Co^{2+}) and Sb^{5+} as a function of cobalt content (*x*). The dotted lines represent the occupations for the case of maximum order for this stoichiometry: $La_2(M)_{2d}(M_{1/3}Sb_{2/3})_{2c}O_6$.

Table 4
Bond distances and bond angles for the octahedral sites 2*d* and 2*c* of $La_2Ni_{4/3-x}Co_xSb_{2/3}O_6$ obtained from NPD refinements. Each distance has multiplicity of 2. Θ is B_{2d}–O–B_{2c} angle.

x	*T* (K)	Distances (Å)		Θ (°)
		B_{2d}–O	B_{2c}–O	
0	300	2.080(3)	2.005(4)	153.2(1)
		2.065(3)	2.012(3)	154.2(2)
		2.042(5)	2.019(5)	155.0(2)
	3	2.057(4)	2.019(4)	153.5(2)
		2.056(4)	2.021(4)	153.4(2)
		2.037(4)	2.021(4)	154.3(2)
1/3	300	2.079(4)	2.018(4)	152.0(2)
		2.056(4)	2.015(4)	155.0(2)
		2.048(6)	2.019(6)	154.5(2)
	3	2.012(4)	2.066(4)	153.6(2)
		2.009(5)	2.073(4)	153.2(2)
		2.039(7)	2.023(7)	154.2(3)
2/3	300	2.064(4)	2.041(4)	151.5(2)
		2.046(4)	2.029(4)	155.1(2)
		2.01(1)	2.07(1)	154.1(4)
	3	2.063(4)	2.039(4)	151.4(2)
		2.045(4)	2.027(4)	155.0(2)
		2.01(1)	2.05(1)	153.7(5)
1	300	2.113(5)	1.1999(5)	151.3(2)
		2.091(5)	1.991(5)	154.8(2)
		2.091(8)	1.981(8)	154.4(3)
	3	2.113(5)	1.999(5)	151.0(2)
		2.091(5)	1.991(5)	154.7(2)
		2.091(8)	1.981(8)	153.6(3)

First, it is observed a step like or double hysteresis behavior at low fields in all cobalt perovskites. At 5 K these steps are very noticeable, at 15 K they almost disappear and at 20 K they are completely absent, as it can be seen for $La_2NiCo_{1/3}Sb_{2/3}O_6$ in Fig. 8.

Double hysteresis has been observed for example in nanoscopic samples with two ferromagnetic phases and different coercive fields [26,27]. A combination of interacting softer and harder magnetic phases is required in the material to produce such a step like behavior in magnetization loops. In double perovskites $La_2Ni_{4/3-x}Co_{1/3}Sb_{2/3}O_6$ there could be two magnetic phases: one corresponding to Ni^{2+} ions and other to Co^{2+}. However the step like behavior is observed even for $x=4/3$, as it was previously reported [19] and not observed for $x=0$. So, in this scenario both, softer and harder magnetic phases, must be intrinsically related to the Co^{2+} ion.

Phenomena like double hysteresis and multiple steps in *M* vs. *H* curves were found in doped cobaltites $Ga_{1-x}Ca_xBaCo_2O_{5.5}$ [28] and $EuBaCo_{2-x}M_xO_{5.5}$ with $M^{2+}=Zn^{2+}$, Cu^{2+} [29] and $M^{2+}=Ni^{2+}$ [30]. In undoped samples all cobalt ions are Co^{3+}, and the replacement of Ga^{3+} for Ca^{2+} in the first case and Co^{3+} for Zn^{2+}, Cu^{2+} or Ni^{2+} in the second case produce the oxidation of some amount of Co^{3+} to Co^{4+}. This mixture of $Co^{3+/4+}$ and the multiple spin states of them – low, intermediate and high – results in the coexistence of ferromagnetic zones in a ferro or antiferromagnetic matrix, and this causes the emergence of steps in hysteresis loops, also related to structural distortions.

In $La_2Ni_{4/3-x}Co_xSb_{2/3}O_6$ the increase in cobalt content (*x*) expands the unit cell, Fig. 3, but it does not produce further structural distortions. This can be seen in bond angles, Table 4, which are very similar among the family, and in mean octahedral distortions calculated from *B*–O distances (not shown), also similar for all compositions. On the other hand, from charge balance and synthesis conditions we expect all cobalt ions to be 2+, a state with no intermediate spin configuration. Therefore, the presence of multiple spin states requires the oxidation of Co^{2+} and the reduction of another ion, and the one that can do this is Sb^{5+} to Sb^{3+}. However, Sb^{3+} is rarely found in ceramics, in fact there is not – to our knowledge – any perovskite with Sb^{3+}; then we disregard the presence of $Co^{3+/4+}$.

The saturation M_s and the coercive fields H_C for cobalt perovskites point out an alternative explanation for the double hysteresis: the loops recorded up to ± 50 kOe at 5 K are minor loops. Looking at the high field zone in Fig. 7, where it is expected – if the field is large enough – to reach saturation, while $La_2Ni_{4/3}Sb_{2/3}O_6$ at 10 kOe is almost saturated and in the reversible region, the other compositions – even at 50 kOe – show a low increase in magnetization, and then we cannot obtain the experimental M_s. Besides, the double perovskites with cobalt show irreversibility up to ± 50 kOe.

However, some estimation can be made in order to obtain microscopic information. For a ferromagnetic order the theoretical

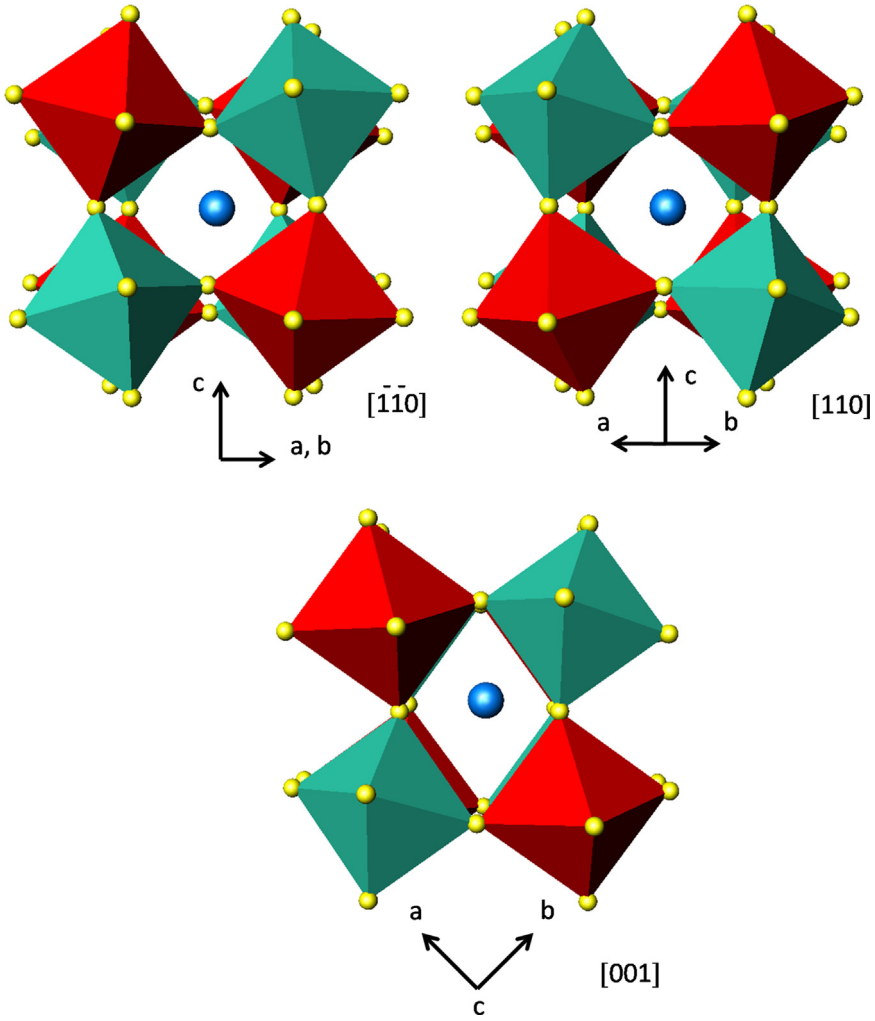

Fig. 5. Monoclinic structure of double perovskites $La_2Ni_{4/3-x}Co_xSb_{2/3}O_6$ along [$\bar{1}$1 0], [110] and [001] directions. Red octahedra: $B_{2d}O_6$, turquoise octahedra: $B_{2c}O_6$, yellow spheres: O^{2-}, blue spheres: La^{3+}. (For interpretation of the references to color in this figure caption, the reader is referred to the web version of this article.)

Table 5
Bond valence sums at 300 and 3 K for all sites of double perovskites $La_2Ni_{4/3-x}Co_xSb_{2/3}O_6$ where $x=0$, 1/3, 2/3 and 1, obtained from Rietveld refinements of powder neutron diffraction data.

Sample	Atom	Site	Bond valence sums		
			Expected	300 K	3 K
$La_2Ni_{4/3}Sb_{2/3}O_6$	La	4*e*	3	2.90(2)	2.96(2)
$x=0$	B	2*d*	2.1	2.1	2.1
	B	2*c*	3.9	4.0	3.9
	O	4*e*	2	1.97(1)	1.97(1)
	O	4*e*	2	1.97(1)	1.99(1)
	O	4*e*	2	1.98(1)	2.01(1)
$La_2NiCo_{1/3}Sb_{2/3}O_6$	La	4*e*	3	2.90(2)	2.94(2)
$x=1/3$	B	2*d*	2.1	2.1	2.4
	B	2*c*	3.9	4.0	3.6
	O	4*e*	2	1.97(2)	1.94(1)
	O	4*e*	2	1.96(1)	1.96(1)
	O	4*e*	2	2.01(1)	2.02(1)
$La_2Ni_{2/3}Co_{2/3}Sb_{2/3}O_6$	La	4*e*	3	2.89(2)	2.94(2)
$x=2/3$	B	2*d*	2.05	2.3	2.3
	B	2*c*	3.95	3.7	3.8
	O	4*e*	2	1.94(1)	1.96(1)
	O	4*e*	2	1.97(1)	1.98(1)
	O	4*e*	2	1.99(2)	2.02(2)
$La_2Ni_{1/3}CoSb_{2/3}O_6$	La	4*e*	3	2.89(2)	2.95(2)
$x=1$	B	2*d*	2.04	2.0	2.0
	B	2*c*	3.96	4.3	4.3
	O	4*e*	2	2.05(2)	2.06(2)
	O	4*e*	2	1.95(1)	1.97(1)
	O	4*e*	2	2.05(2)	2.08(2)

saturation magnetization for these samples is $M_{s-ferro} = [2(4/3-x)+3x]\mu_B/f.u.$, where x is the cobalt content and we take into account the contribution of Ni^{2+} and Co^{2+} (HS) configuration, with 2 and 3 unpaired electrons respectively. The obtained values are drawn in Fig. 7, and are much bigger than the experimental magnetization at 50 kOe for each sample. Another approach is to estimate the saturation taking into account the crystallographic data obtained before and the magnetic interactions in the system.

Nearest neighbors interaction (nn) between two magnetic ions is M_{2d}–O–M_{2c}, where $M^{2+} = Ni^{2+}$ or Co^{2+}, at approximately 4.1 Å, Table 4. This superexchange interaction is antiferromagnetic according to Goodenough–Kanamori rules [12]. Fig. 9(a) shows a 2D representation of the distribution of transition metals M^{2+} and Sb^{5+} ions over the octahedral sites in the case of maximum order, and also nearest neighbor (nn), next nearest neighbor (nnn) and third nearest neighbor (tnn) interactions. Due to the 2/1 proportion of M^{2+}/Sb^{5+} there are many M_{2d}–O–M_{2c} paths and if we consider that nn prevails over nnn and tnn, we can consider two magnetic sub-nets, 2*d* and 2*c*, antiferromagnetically coupled, being the system ferrimagnetic because there is not a total cancellation of the magnetization, Fig. 9(b). The ferrimagnetic theoretical saturation is given as the difference between the magnetization of each sub-net: $M_{s-ferri} = m_{2d} - m_{2c}$. For each f.u., and from occupation fractions *O* of Table 3,

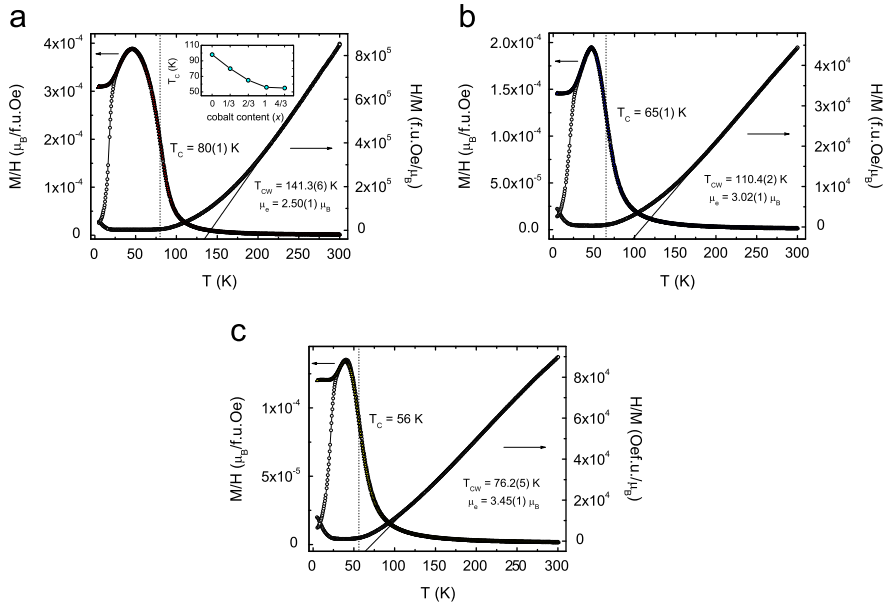

Fig. 6. *M/H* (left axis) and *H/M* (right axis) vs. *T* for: (a) $La_2NiCo_{1/3}Sb_{2/3}O_6$, $x=1/3$, (b) $La_2Ni_{2/3}Co_{2/3}Sb_{2/3}O_6$, $x=2/3$, and (c) $La_2Ni_{1/3}CoSb_{2/3}O_6$, $x=1$. The measurements were performed at 1 kOe under zero field (open circles) and field cooling (color triangles) conditions. Black lines are the fits obtained in the 200–300 K zone with the Curie–Weiss law for ZFC data. Obtained Curie–Weiss temperature T_{CW} and effective magnetic moment μ_e are indicated for each sample. Vertical dotted lines are the Curie temperatures T_C, taken as the minima in dM/dT vs. *T* curves. The evolution of T_C with cobalt content (x) is shown in the inset of (a); data for $x=0$ and 4/3 were taken from [17,18] and [19] respectively.

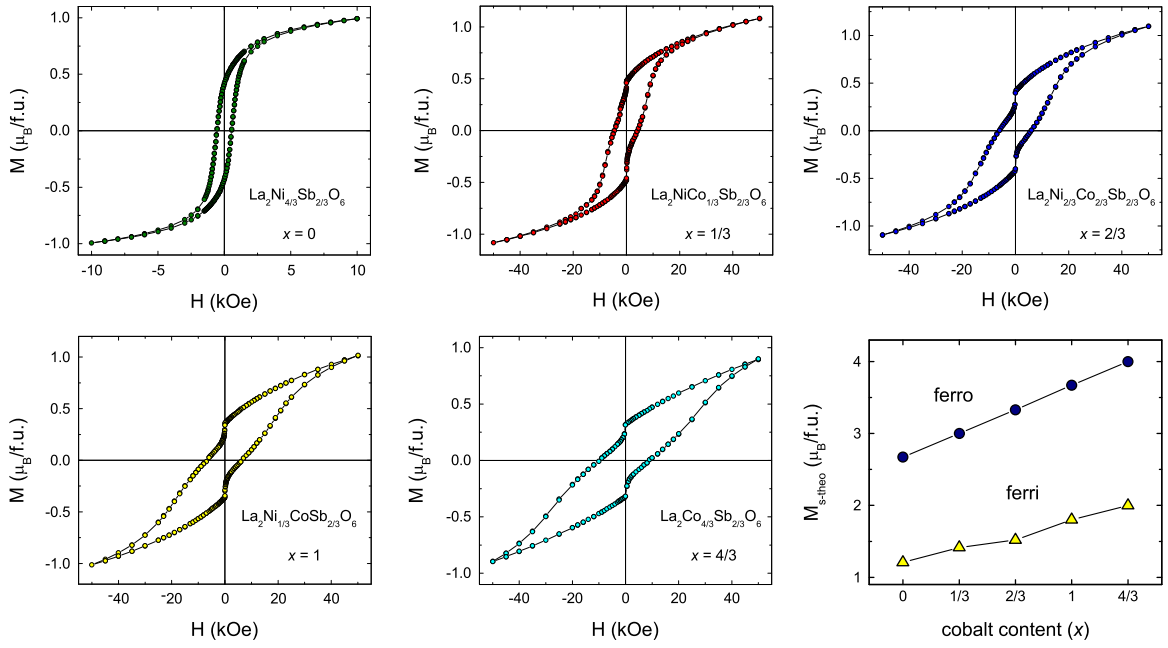

Fig. 7. Hysteresis loops at 5 K taken under ZFC for $La_2Ni_{4/3-x}Co_xSb_{2/3}O_6$, where $x=0$, 1/3, 2/3, 1 and 4/3. Dependence of the theoretical magnetic saturation M_{s-theo} with cobalt content (x) for a ferromagnetic (ferro) and a ferrimagnetic (ferri) order is shown in the last graph. For details of the calculations, see the text.

$m_y = 2 \times (2\mu_B O_{Ni_y^{2+}} + 3\mu_B O_{Co_y^{2+}})$, where $y=2d$ or $2c$. The results are shown in Fig. 7, where it is observed that $M_{s-ferri}$ increases, just like $M_{s-ferro}$ do, with cobalt doping (x), but the values are lower than $M_{s-ferro}$ and closer to the magnetizations reached at the highest experimentally accessible field. Then, the samples have an antiferromagnetic order with a net magnetization, that is, a ferrimagnetic one.

Concerning the fields for which the magnetization is zero $H(M=0)$, $La_2Ni_{4/3}Sb_{2/3}O_6$ at 5 K has $H^+(M=0) = -H^-(M=0)$, where we use superscripts + and − to differentiate the values obtained from the superior and inferior branch of the loop respectively. The double perovskites with $x=1/3$, 2/3, 1 and 4/3 at 5 K have $H^+(M=0) \neq -H^-(M=0)$, while the remanent magnetizations $M^+_{rem} = -M^-_{rem}$ for all compositions. As we show in Fig. 10 $H(M=0)$ and M_{rem} depend on the maximum field achieved in the hysteresis loops. This makes evident that the loops at 5 K up to ±50 kOe in $La_2Ni_{4/3-x}Co_xSb_{2/3}O_6$ with $x=1/3$, 2/3 and 1 are minor loops. Therefore $H(M=0)$ and M_{rem} are not equivalent to the coercive field H_C and the remanent magnetization of the samples. This fact was also reported for $La_2Co_{4/3}Sb_{2/3}O_6$ [19].

Higher fields would be necessary to reach saturation, or at least a reversible M vs. H region, to measure the major loop and have $H(M=0)=H_C$. Usually for a ferro/ferrimagnetic material the saturation decreases as temperature increases, so at higher temperatures than 5 K we would be able to saturate the system or to reach a reversible M vs. H region within our ±50 kOe accessible experimental region. $H(M=0)$ at 5 and 15 K are presented in Table 6, obtained from hysteresis loops. The asymmetry at 5 K is very high, while at 15 K it is not present. Consequently at 15 K and above we can access to coercive fields H_C. Inset of Fig. 8 shows H_C vs. cobalt content (x) at 15 K, where a noticeable hardening effect is observed as cobalt content increases.

The need of high magnetic fields to obtain major loops in cobalt compounds has been reported for $La_{1-x}Sr_xCoO_3$ [31], where at 3 K even the hysteresis loops taken up to ±80 kOe have an horizontal shift, attributed to the exchange coupling between *spin glass* regions and ferromagnetic clusters.

An indication of magnetic frustration in our samples is found at 5 K in the initial (or virgin) curve of M vs. H recorded after ZFC. For all cobalt perovskites we found that the initial curve lays outside the inferior branch of the loop, Fig. 11, in the same way as was reported previously for $x=0$ composition [17,18]. This effect has been observed in different disordered magnetic systems, including perovskite systems like $La_{0.47}Ce_{0.20}Ca_{0.33}MnO_3$ [32] and $LaMn_{0.85}Cr_{0.15}O_{3+\delta}$ [33], where the phenomenon was related to cationic disorder, which leads to the coexistence of different magnetic interactions, and a *spin glass* behavior. In our samples the use of a demagnetizing procedure (consisting in putting the sample at 50 kOe and then slowly oscillating the field with decreasing amplitude down to zero) allows to reach a zero magnetization state, but

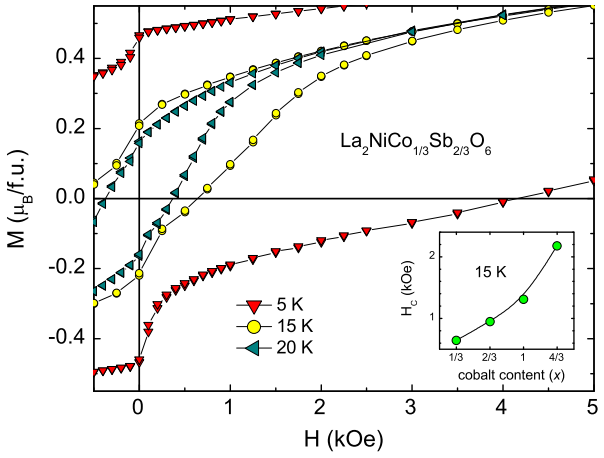

Fig. 8. Details of the low field zone of M vs. H for $La_2NiCo_{1/3}Sb_{2/3}O_6$ measured at three temperatures and in ZFC conditions. The inset shows the evolution of the coercive field H_C with cobalt content (x) at 15 K. The line is a guide to the eye.

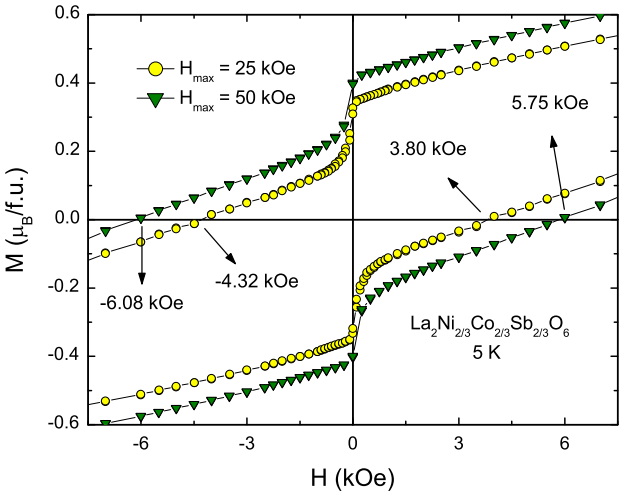

Fig. 10. Details of hysteresis loops at 5 K for $La_2Ni_{2/3}Co_{2/3}Sb_{2/3}O_6$ obtained up to ±25 kOe (circles) and up to ±50 kOe (triangles).

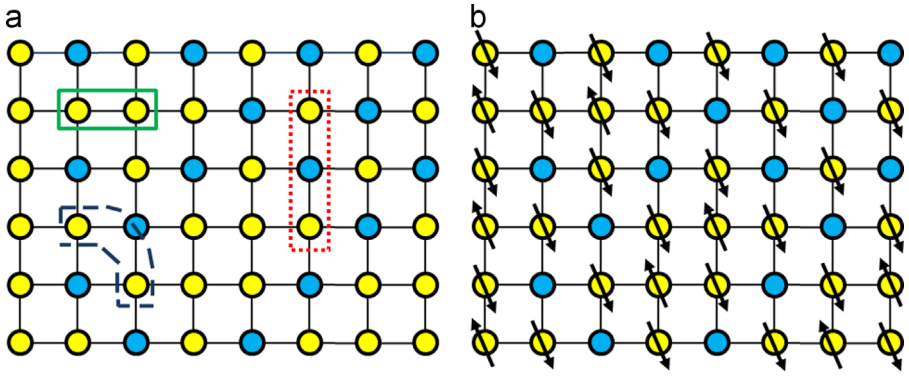

Fig. 9. (a) 2D distribution of M^{2+} (yellow circles) and Sb^{5+} (cyan circles) over two sites in double perovskites $La_2M_{4/3}Sb_{2/3}O_6$, where M^{2+} is $Ni^{2+}+Co^{2+}$. A maximum order situation is plotted, a square structure has been supposed and La^{3+} and O^{2-} ions were omitted. Nearest neighbor (nn, green line), next nearest neighbor (nnn, dash blue line) and third nearest neighbor (tnn, dot red line) interactions are depicted. (b) Possible spin arrangement if antiferromagnetic superexchange interaction at nn (M^{2+}–O–M^{2+}) dominates over nnn and tnn. For simplicity all arrows were drawn with the same modulus. (For interpretation of the references to color in this figure caption, the reader is referred to the web version of this article.)

Table 6
$H(M=0)$ from M vs. H curves for $La_2Ni_{4/3-x}Co_xSb_{2/3}O_6$ double perovskites with $x=1/3$, 2/3 and 1. In each column the left and right numbers indicate the values obtained from the superior and inferior branches of hysteresis loop respectively.

T (K)	$H(M=0)$ (kOe)		
	$x=1/3$	$x=2/3$	$x=1$
5	−4.62/4.14	−6.15/5.80	−6.76/6.42
15	−0.65/0.64	−0.96/0.94	−1.32/1.31

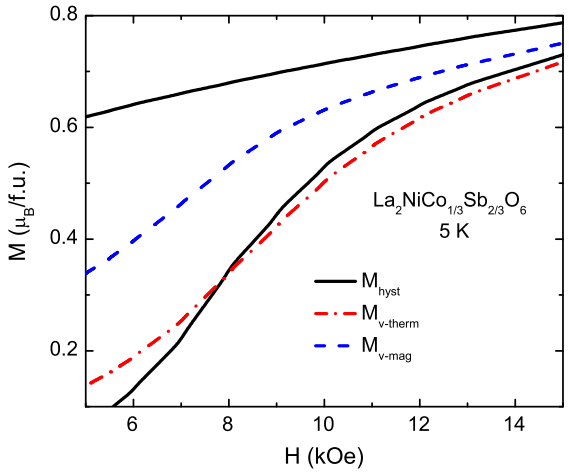

Fig. 11. Virgin curve after thermal demagnetization ($M_{v-therm}$, dash-dot line) and the corresponding hysteresis loop obtained after 50 kOe was reached (M_{hyst}, continuous line) for $La_2NiCo_{1/3}Sb_{2/3}O_6$ at 5 K. The virgin curve obtained after a demagnetization process at 5 K is also shown (M_{v-mag}, dash line).

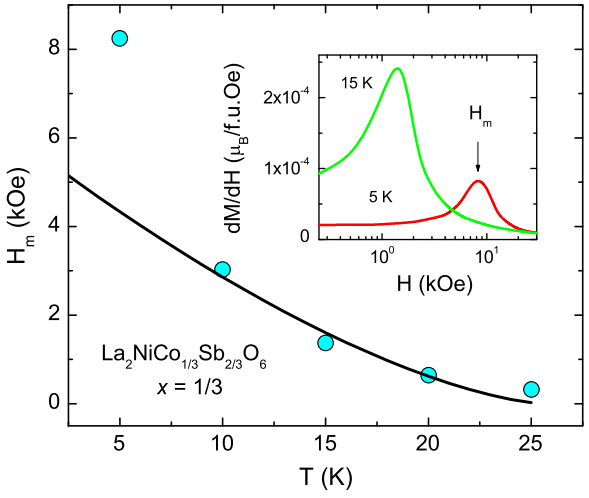

Fig. 12. H_m vs. T for $La_2NiCo_{1/3}Sb_{2/3}O_6$, where H_m is the field of the maximum in dM/dH vs. T curve (see inset). The line is a fit obtained with the de Almeida–Thouless model: $H_m=H_0(1-T/T_f)^{3/2}$.

this state is different from the magnetic state obtained by cooling the sample in a zero field, as can be seen in Fig. 11: the virgin curve after a magnetic demagnetization lies inside the hysteresis loop, unlike the virgin curve measured after thermal demagnetization (that is, cooling the sample in the zero field). Then, a demagnetizing protocol seems to overcome the frustration.

The inset of Fig. 12 shows the virgin magnetization curve derivative dM/dH vs. T at two different temperatures for $La_2NiCo_{1/3}Sb_{2/3}O_6$, where a clear maximum H_m is observed, related to a characteristic magnetic field to spin alignment. There are several scenarios that may describe the temperature dependence of H_m. Generally speaking we could write a power law of the form $H_m=H_0\,(1-T/T_f)^a$, where T_f is the freezing temperature. For a *spin glass* system $H_m(T)$ represents the line that separates the vitreous and the ferro/ferrimagnetic ordered state. For the de Almeida–Thouless model $a=3/2$ [34], while for a Gabay–Toulouse scenario $a=2/3$ [35]. In the case of a metamagnetic transition $a=1/2$, like as it was reported for ilmenite $FeTiO_3$ [36]. Our experimental data for $La_2NiCo_{1/3}Sb_{2/3}O_6$, Fig. 12, is not well described by the two latter cases, but the de Almeida–Thouless model seems to fit well the data between 10 and 25 K, with $H_0=3.7(6)$ kOe and $T_f=30(2)$ K, close to the temperature where the divergence between M_{ZFC} and M_{FC} occurs, Fig. 6. Clearly $H_m(5\text{ K})$ is out of the de Almeida–Thouless line, indicating a drastic change of regime.

Frustration at low temperatures in double perovskites $La_2Ni_{4/3-x}Co_xSb_{2/3}O_6$ can arise due to the competition of different magnetic interactions. According to Table 4 the distances between nn, nnn and tnn, Fig. 9(a), are approximately 4.08, 6.96 and 8.16 Å respectively. At high temperature nn interactions prevail over nnn and tnn interactions, and those are responsible for the magnetic transition. But when the temperature is lowered down to $\sim$30 K, nnn and tnn interactions become important and the three types of interactions compete; frustration appears because all the interactions are antiferromagnetic and impossible to satisfy at the same time. Therefore frustrated regions are expected, depending on the microscopic distribution of Ni^{2+}, Co^{2+} and Sb^{5+}.

The fact that nnn and tnn interactions become important at low temperatures is well established for a wide number of double perovskites of the type $A_2BB'O_6$ where only B is a magnetic ion and order between B and B' is very high. Under these conditions only nnn and tnn interactions are possible and for this kind of materials antiferromagnetic transitions are observed below 30 K: Sr_2MnTeO_6 [37], $LaSrMnNbO_6$ [38], La_2CoTiO_6 and La_2NiTiO_6 [39], $LaBaTaNiO_6$ and $LaBaTaCoO_6$ [40], $LaPbMSbO_6$ where M=Mn, Co and Ni [41], among others.

The frustration is present in all samples but it is interesting to note the dominant effect of cobalt ions over magnetic properties: for $La_2Ni_{4/3}Sb_{2/3}O_6$ thermal evolution of H_m could not be explained in base to none of the mechanism described above [17,18]. On the other hand the sample with the minimum cobalt content $La_2NiCo_{1/3}Sb_{2/3}O_6$ changes the type of dependence and follows the de Almeida–Thouless line.

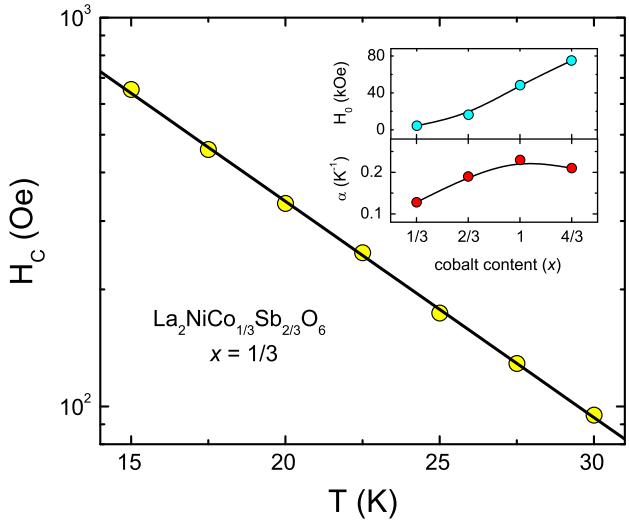

Fig. 13. H_C vs. T for $La_2NiCo_{1/3}Sb_{2/3}O_6$. Yellow circles are experimental data and black line the fit obtained with a cluster model: $H_C=H_0e^{-\alpha T}$. The obtained H_0 and α values are shown as a function of cobalt content (x) in the inset, lines are guide to the eye. Values for $x=4/3$ were taken from [19]. (For interpretation of the references to color in this figure caption, the reader is referred to the web version of this article.)

The analysis of the thermal evolution of H_C can give us additional information. For $La_2Ni_{4/3}Sb_{2/3}O_6$ two different regimes were found, both of them power laws $H_C(T)^{1/\beta} = cT/T_0$ [17,18], where c is a constant. This kind of evolution is typical from thermally activated domain wall movement [42]. On the other hand $La_2Co_{4/3}Sb_{2/3}O_6$ follows an exponential dependence $H_C(T) = H_0 e^{-\alpha T}$ [19], where α is related to the volume of magnetic clusters and also with anisotropy. Oxide systems like hemoilmenites $(x)FeTiO_3(1-x)Fe_2O_3$ [43] and $La_{1-x}Sr_xCoO_3$ [44] also follow this exponential dependence. H_C vs. T for $x=1/3$, 2/3 and 1 are not well described by a power law, even $La_2NiCo_{1/3}Sb_{2/3}O_6$, proving again that with a small amount of cobalt the magnetic behavior changes drastically. $x=1/3$, 2/3 and 1 samples have an exponential dependence, shown in Fig. 13 for $x=1/3$, suggesting the presence of magnetic clusters as a consequence of the magnetic frustration stated before. α increases with cobalt doping, as well as H_0, inset in Fig. 13.

4. Conclusions

$La_2Ni_{4/3-x}Co_xSb_{2/3}O_6$ with $x=0$, 1/3, 2/3, 1 and 4/3 were synthesized by the solid state method. X-ray and neutron diffraction data for $x=0$, 1/3, 2/3, 1 show that all samples crystallize in the monoclinic space group $P2_1/n$ and the cell parameters a, b and c increase as cobalt content increases. The order among octahedral 2d and 2c sites is almost perfect for all compositions, with 2d site nearly occupied by transition metals only and 2c site with all Sb^{5+} randomly distributed.

Magnetization vs. temperature curves show an ordered state below T_C, where T_C decreases as cobalt content increases, from 98 to 55 K for $x=0$ and 4/3 respectively. These magnetic transitions are attributed to nearest neighbor interactions (nn), superexchange M^{2+}–O–M^{2+}. The maximum magnetization values for $La_2Ni_{4/3-x}Co_xSb_{2/3}O_6$ extracted from magnetization vs. applied field curves at 5 K correlate with the expected values for a ferrimagnetic system. Below 30 K a frustrated state appears for all samples due to the competition between nn, nnn and tnn interactions. For $x=0$ thermal evolution of H_m, obtained as the inflection point in virgin magnetization curves, does not follow any power law, and the thermal dependence of coercive field H_C is well described by domain wall movement mechanisms. Instead, for the Co^{2+} double perovskites H_m vs. T fit the de Almeida–Thouless line and H_C vs. T follow an exponential dependence, evidencing spin glass like behavior.

5. Supplementary information

Structural information extracted from crystal structure refinements of powder neutron diffraction data for $La_2Ni_{4/3-x}Co_xSb_{2/3}O_6$with x = 0, 1/3, 2/3 and 1 have been deposited at the ICSD Fachinformationszentrum Karlsruhe (FIZ) (E-mail: CrysDATA@FIZ-Karlsruhe.DE). ICSD files numbers are: for $La_2Ni_{4/3}Sb_{2/3}O_6$426191 (300 K) and 426192 (3 K); for $La_2NiCo_{1/3}Sb_{2/3}O_6$ 426189 (300 K) and 426190 (3 K); for $La_2Ni_{2/3}Co_{2/3}Sb_{2/3}O_6$426187 (300 K) and 426188 (3 K); for $La_2Ni_{1/3}CoSb_{2/3}O_6$426185 (300 K) and 426186 (3 K).

Acknowledgments

D.G.F. thanks CONICET for fellowship. R.E.C. thanks FONCYT for PICT2007-303, CONICET for PIP #11220090100995 and SECyT-UNC for the Project 162/12. G.N. thanks ANPCyT PICT2007-819, CONICET for PIP #11220090100448 and SeCTyP-UNCuyo 06/C313. We gratefully acknowledge Institut Laue Langevin (ILL), Grenoble, France, for access to D2B line.

References

[1] G.H. Jonker, J.H. Van Santen, Physica 16 (3) (1950) 337–349.
[2] J. Longo, R. Ward, J. Am. Chem. Soc. 83 (13) (1961) 2816–2818.
[3] F.K. Patterson, C.W. Moeller, R. Ward, Inorg. Chem. 2 (1) (1963) 196–198.
[4] J.G. Bednorz, K.A. Muller, Z. Phys. B: Condens. Matter 64 (2) (1986) 189–193.
[5] S. Jin, T.H. Tiefel, M. McCormack, R.A. Fastnacht, R. Ramesh, L.H. Chen, Science 264 (5157) (1994) 413–415.
[6] K.-I. Kobayashi, T. Kimura, H. Sawada, K. Terakura, Y. Tokura, Nature 395 (6703) (1998) 677–680.
[7] G. King, P.M. Woodward, J. Mater. Chem. 20 (2010) 5785–5796.
[8] P.K. Davies, H. Wu, A.Y. Borisevich, I.E. Molodetsky, L. Farber, Annu. Rev. Mater. Res. 38 (2008) 369–401.
[9] D.D. Sarma, Curr. Opin. Solid State Mater. Sci. 5 (2001) 261–268.
[10] J.-S. Zhou, J.B. Goodenough, Phys. Rev. Lett. 96 (2006) 247202.
[11] V.C. Fuertes, M.C. Blanco, D.G. Franco, J.M. de Paoli, R.D. Sánchez, R.E. Carbonio, Mater. Res. Bull. 46 (2011) 62–69.
[12] J.B. Goodenough, Magnetism and the Chemical Bond, John Wiley & Sons, 1966.
[13] L. Ortega-San Martin, J.P. Chapman, L. Lezama, J.J. Saiz Garitaonandia, J. Sánchez Marcos, J. Rodríguez-Fernández, M.I. Arriortua, T. Rojo, J. Mater. Chem. 16 (2006) 66–76.
[14] S.A. Ivanov, P. Nordblad, R. Tellgren, A. Hewat, Mater. Res. Bull. 44 (2009) 822–830.
[15] T.C. Gibb, R.J. Whitehead, J. Mater. Chem. 3 (6) (1993) 591–596.
[16] T.C. Gibb, J. Mater. Chem. 3 (5) (1993) 441–446.
[17] D.G. Franco, R.E. Carbonio, G. Nieva, IEEE Trans. Magn. 49 (8) (2013) 4656–4659.
[18] D.G. Franco, R.E. Carbonio, E.E. Kaul, G. Nieva, J. Magn. Magn. Mater. 346 (2013) 196–202.
[19] D.G. Franco, V.C. Fuertes, M.C. Blanco, M.T. Fernández-Díaz, R.D. Sánchez, R.E. Carbonio, J. Solid State Chem. 194 (2012) 385–391.
[20] H.M. Rietveld, J. Appl. Crystallogr. 2 (1969) 65–71.
[21] J. Rodriguez-Carvajal, Physica B 192 (1993) 55–69.
[22] I. Alvarez, M.L. Veiga, C. Pico, Solid State Ionics 91 (1996) 265–271.
[23] M.T. Anderson, K.B. Greenwood, G.A. Taylor, K.R. Poeppelmeier, Prog. Solid State Chem. 22 (1993) 197–233.
[24] R.D. Shannon, Acta Crystallogr. Sect. A 32 (1976) 751–767.
[25] I.D. Brown, in: M. OKeeffe, A. Navrotsky (Eds.), Structure and Bonding in Crystals, vol. 1, Academic Press, New York, 1981.
[26] E.E. Fullerton, J.S. Jiang, S.D. Bader, J. Magn. Magn. Mater. 200 (1999) 392–404.
[27] H. Zeng, J. Li, Z.L. Wang, S. Sun, Nature 420 (6914) (2002) 395–398.
[28] N. Thirumurugan, A. Bharathi, A. Arulraj, C.S. Sundar, Mater. Res. Bull. 47 (2012) 941–946.
[29] B. Raveau, Ch. Simon, V. Caignaert, V. Pralong, F.-X. Lefevre, J. Phys.: Condens. Matter 18 (2006) 10237–10247.
[30] B. Raveau, Ch. Simon, V. Pralong, V. Caignaert, F.-X. Lefevre, Solid State Commun. 139 (2006) 301–305.
[31] S. Yuan, K. Xu, Z. Li, L. Yu, B. Kang, S. Cao, J. Appl. Phys. 105 (2009) 093910.
[32] G. Alejandro, D.G. Lamas, L.B. Steren, J.E. Gayone, G. Zampieri, A. Caneiro, M.T. Causa, M. Tovar, Phys. Rev. B 67 (2003) 064424.
[33] L.B. Morales, R. Zysler, A. Caneiro, J. Solid State Chem. 181 (2008) 1824–1832.
[34] J.R.L. de Almeida, D.J. Thouless, J. Phys. A: Math. Gen. 11 (5) (1978) 983–990.
[35] M. Gabay, G. Toulouse, Phys. Rev. Lett. 47 (3) (1981) 201–204.
[36] H. Kato, M. Yamada, H. Yamauchi, H. Hiroyoshi, H. Takei, H. Watanabe, J. Phys. Soc. Jpn. 51 (6) (1982) 1769–1777.
[37] L. Ortega-San Martín, J.P. Chapman, L. Lezama, J. Sánchez Marcos, J. Rodríguez-Fernández, M.I. Arriortua, T. Rojo, Eur. J. Inorg. Chem. 7 (2006) 1362–1370.
[38] T. Yang, T. Perkisas, J. Hadermann, M. Croft, A. Ignatov, M. Greenblatt, J. Solid State Chem. 183 (2010) 2689–2694.
[39] E. Rodríguez, M.L. López, J. Campo, M.L. Veiga, C. Pico, J. Mater. Chem. 12 (2002) 2798–2802.
[40] S.L. Samal, T. Magdaleno, K.V. Ramanujachary, S.E. Lofland, A.K. Ganguli, Solid State Sci. 12 (2010) 1382–1386.
[41] D.G. Franco, R.E. Carbonio, G. Nieva, IEEE Trans. Magn. 49 (8) (2013) 4594–4597.
[42] J.I. Arnaudas, A. Del Moral, P.A.J. De Groot, J. Magn. Magn. Mater. 104–107 (1992) 115–116.
[43] M. Charilaou, J.F. Loffler, A.U. Gehring, Phys. Rev. B 83 (2011) 224414.
[44] S. Mukherjee, R. Ranganathan, P. Mondal, J. Phys. Chem. Solids 61 (2000) 1433–1438.